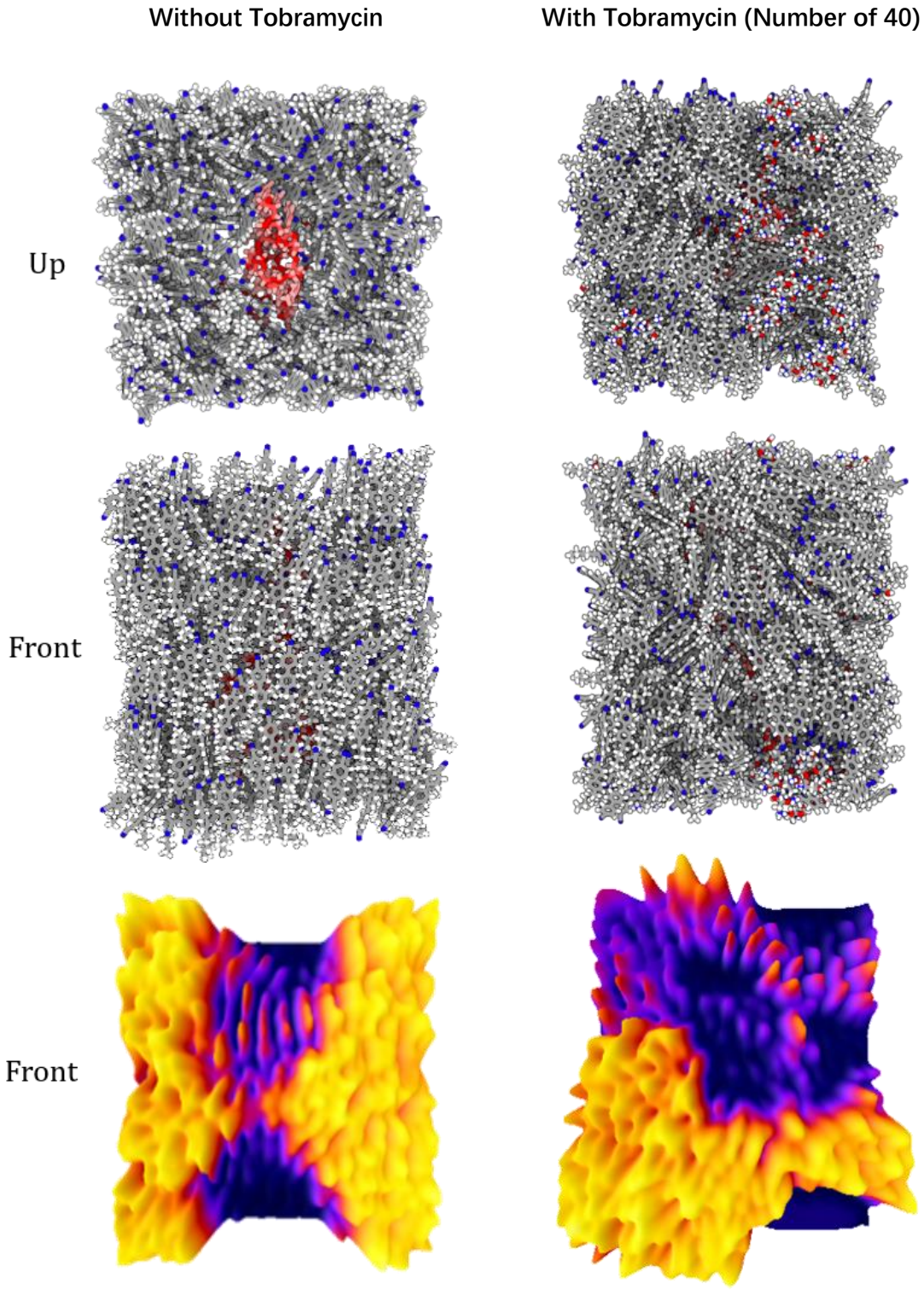
Without Tobramycin
With Tobramycin (Number of 40)
Up
Front
Front

Molecular Dynamics Simulation as a Promising Approach for Computational Study of Liquid Crystal-based Aptasensors

Hamed Zahraee[a,b,c], Zahra Khoshbin[a,b,c,*], Seyed Mohammad Taghdisi[a,d], Khalil Abnous[b,c,*]

[a] *Targeted Drug Delivery Research Center, Pharmaceutical Technology Institute, Mashhad University of Medical Sciences, Mashhad, Iran*

[b] *Pharmaceutical Research Center, Pharmaceutical Technology Institute, Mashhad University of Medical Sciences, Mashhad, Iran*

[c] *Department of Medicinal Chemistry, School of Pharmacy, Mashhad University of Medical Sciences, Mashhad, Iran*

[d] *Department of Pharmaceutical Biotechnology, School of Pharmacy, Mashhad University of Medical Sciences, Mashhad, Iran*

* Corresponding Authors

Prof. Khalil Abnous; E-mail address: abnouskh@mums.ac.ir

Dr. Zahra Khoshbin; E-mail address: khoshbinz991@mums.ac.ir

Abstract

As a potent computational methodology, molecular dynamics (MD) simulation provides advantageous knowledge about biological compounds from the molecular viewpoint. In particular, MD simulation gives exact information about aptamer strands, such as the short synthetic oligomers, their orientation, binding sites, folding-unfolding state, and conformational re-arrangement. Also, the effect of the different chemicals and biochemicals as the components of aptamer-based sensors (aptasensors) on the aptamer-target interaction can be investigated by MD simulation. Liquid crystals (LCs) as soft substances with characteristics of both solid anisotropy and liquid fluidity are new candidates for designing label-free aptasensors. To now, diverse aptasensors have been developed experimentally based on the optical anisotropy, fluidity, and long-range orientational order of LCs. Here, we represent a computational design of an LC-based aptasensor through a detailed MD simulation study. The different parameters are defined and studied to achieve a comprehensive understanding of the computational design of the LC-based aptasensor, including the density of LCs, their orientation angle, and lognormal distribution in the absence and presence of aptamer strands, both aptamer and target molecules with various concentrations, and interfering substance. As a case study, the tobramycin antibiotic is considered the target molecule for the computational design of the LC-based aptasensor.

Keywords: Aptamer; Liquid crystal; Biosensor; MD simulation; Tobramycin; Density

1. Introduction

Today, biosensors as efficient analytical devices have gained specific attention for applying in different fields of science, including healthcare, pharmaceuticals, clinical diagnostics, environmental monitoring, and food quality control [1, 2]. Generally, biosensors can include diverse types of bioreceptor segments for the special grafting to targets, such as antibodies, peptides, nucleic acids, cells, enzymes, aptamers, etc. Among them, biosensors based on aptamers (defined as aptasensors) are the greatest well-organized biosensing tools [3]. Aptamers are synthetic single-stranded oligonucleotides with great binding affinity to various targets, screened from systematic evolution of ligands by exponential enrichment (abbreviated as SELEX) selection method. This in-vitro production method eliminates the requirement for laboratory animals to synthesize aptamers. The low weight and small size of aptamers makes their generation and modification facile and cost-effective. Aptamers possess long shelf life, less immunogenicity and toxicity, great stability, biocompatibility, and reversible thermal denaturation. These outstanding advantages turn aptamers to efficacious bioreceptors for diverse biological sensing approaches. Besides, aptasensors with fast response, low cost, and great target detection limit are user-friendly analytical tools [3-5].

Liquid crystals (LC) as the curious materials with aromatic molecules containing some side chains possess the state between isotropic liquid and crystalline solid. With the features of long-range orientational order, responsiveness to external stimuli, elastic strain, optical anisotropy, and susceptible orientation, LCs have been extensively applied in the field of biosensor design [6, 7]. They are new candidates for optical target detection through visualizing their orientation by a polarized optical microscope [8-11]. Hence, LC-based biosensors are novel for label-free and portable target monitoring assays [12-14].

As a potent computational methodology, molecular dynamics (MD) simulation provides valuable knowledge of biological components [15-21]. Exact information about the direction of aptamers, their binding sites, conformational re-arrangement, and folding-unfolding status can be achieved by MD simulation [22-31]. Besides, the dynamics, structure, and energetics of biological systems can be studied by using MD simulation in accordance with experimental conditions (pressure, pH, temperature, and so on) [32-35]. MD simulation can complement experimental methods by intercepting the wrong interpretations of experimental results [36-39]. Moreover, it can achieve basic information at the atomistic levels when the experimental assays have limitations or are incapable [40-42].

In this study, we emphasize the potency of MD simulation as the complementary or even replacement of experiment assays to design an LC-based aptasensor. Indeed, we represent a

computational design of an LC-based aptasensor through a detailed MD simulation study. As a case study, the tobramycin antibiotic has been chosen as the target molecule. Tobramycin as an anti-infective antibiotic drug commonly utilizes for therapeutic and prophylactic purposes, because of its good water-solubility, low cost, and antimicrobial effects. However, abuse of tobramycin causes adverse problems in human bodies, including neuromuscular blocking, nephrotoxicity, and hypersensitivity [43-45]. To now, some strategies have been applied to determine tobramycin, e.g., high-performance liquid chromatography, UV-Visible absorption spectroscopy, gas chromatography-mass spectrometry, and capillary electrophoresis [46, 47]. Since the methods are time-consuming, high-cost, and operator-dependent, the LC-based aptasensors have been developed for target detection. However, LC-based aptasensors are impaired at much light and high temperatures, due to loss of the LCs' contrast [48, 49]. Hence, we emphasize the potency of MD simulation as the complementary or even replacement of experimental assays to study an LC-based aptasensor. Indeed, MD simulation study of LC-based aptasensors can decrease the cost and time of experimental researches.

2. Computational Details

The crystal structure of tobramycin and specific aptamer was taken from the protein data bank (PDB ID: 1LC4) to construct the MD input files. The sequence of 5´-ACT TGG TTT AGG TAA TGA GTA-3´ was obtained through nucleotide exchange by YASARA software [50] and modification of hydrogen deficiency using PyMOL software (The PyMOL Molecular Graphics System, Version 1.7.2.1 Schrödinger, LLC.) [51]. Since the orientation of LCs can be easily disrupted by aptamer sequences with more than 24 base units [52], two adenosine (A) nucleotides were added to the 3´ end of the aptamer as the spacer. The MD simulations were carried out by GROMACS 2020.2 [53] with the standard CHARMM27 force field [54, 55]. The structure of 5CB LC was drawn by ChemDraw software [56]. Its structural and energetic optimization was done by Chem3D [56] and Gaussian 09 software [57] by DFT (B3LYP) method within the 6-31++G(2d,2p) basis set. The topology parameters for tobramycin and LC were obtained by using SwissParam server [58]. Five rectangular boxes were designed in which the aptamers were fixed on their bottom. One system was considered as the control with no tobramycin molecule. Another box was considered for the interfering system containing 5 gentamycin molecules as the interfering compound. Three others included 5, 20, and 40 tobramycin molecules. The boxes were filled with 450 LC molecules. Charge neutrality was done by adding an adequate number of Na^+ and Cl^- ions to the boxes. The details of the simulated systems is given in Table 1. Simulations were carried out using a cut-off distance of

1.4 nm with a time step of 1 fs. The steepest-descent algorithm [59] was applied to minimize the energy of the system. The velocity rescaling thermostat and Parrinello-Rahman barostat were applied for the temperature and pressure coupling, respectively [60, 61]. Periodic boundary conditions (PBC) were introduced in all directions to implement the MD simulations. Finally, 180 ns production MD simulation of each system was performed with a time step of 1 fs at 300 K. The Particle Mesh Ewald (PME) method was considered to obtain the long-range electrostatic interactions [62].

3. Results and Discussions

To introduce MD simulation as a potent approach for computational design of LC-based aptasensor, five different systems were designed and studied by MD simulation, including 1) control system containing fixed tobramycin aptamer at the bottom of simulation box and LCs, 2) interfering system containing fixed tobramycin aptamer, LCs, and gentamycin molecule, 3) target system 1 containing fixed aptamer, LCs, and 5 tobramycin molecules (named A5T), 4) target system 2 containing fixed aptamer, LCs, and 20 tobramycin molecules (named A20T), and 5) target system 3 containing fixed aptamer, LCs, and 40 tobramycin molecules (named A40T).

The structural stability of the studied systems was investigated by analyzing the root mean square deviation (RMSD). Figure 1A indicates the RMSD plots of the simulated systems, proving that they were in the equilibration state after the MD simulation. Moreover, 180 ns was considered as the proper time for having precise results from further analyses.

Root mean square fluctuation (RMSF) is a criterion for conformational flexibility of DNA strands over the simulation time [63, 64]. The RMSF plot for the aptamer in the absence and presence of the different numbers of tobramycin, and also, in the presence of interfering compound was depicted against the residue numbers during the MD simulation time in Figure 1B. Based on Figure 1B, the aptamer flexibility decreased in some residues with increasing the number of tobramycin in the system, which may be due to more interaction of the aptamer with the target molecules. Figure 1C indicates the frequency of RMSF for the simulated systems in the range of 0.15-0.45 nm.

Figure 2 indicates the situation of the LC molecules in the different simulated systems in the last frame of the MD simulation. Based on Figure 2, LCs were in the same direction with the vertical alignment in the control system free of tobramycin, proving the capability of the aptamer strand with nucleotides lower than 24 to regularly align LCs.

The mean squared displacement (MSD) parameter can reflect the regularity of LCs during the MD simulation. Figure S1 illustrates the remarkable difference in the MSD of the systems in the absence and presence of tobramycin. According to Figure S1, the MSD parameter was higher in the control system; and it decreased with increasing the number of tobramycin in the systems. Thus, a decreased value of the MSD proved the greater irregularity in the vertical orientation of LCs.

To have a detailed insight into the state of the LC molecules for each studied system, their angle changes with respect to the Z axis of the simulation box were investigated. For this purpose, a vertical vector was defined as a basis for the initial state of the LC molecules by considering their C12 and N atoms of the nitrile group (Figure S2); and its angle with the Z axis of the simulation box. Figure 3A indicates the average of the angle of LCs during 180 ns. It is obvious that the changes in the LCs' angle were the least for the control system and system containing gentamycin. Besides, the angle changes for these two systems were the same at the last times of the simulation, proving the negligible disruption of the LCs' alignment in the presence of gentamycin, and also, insignificant interaction of gentamycin with the aptamer. Figure 3A illustrates that the average of the angle increased with enhancing the number of tobramycin molecules. It proves more changes in the vertical alignment of LCs due to the great specific interaction of the aptamer with the target. Figure 3B displays the probability of the angles during the MD simulation. The results highlight that the maximum probability was less than 30° in the control system and system containing gentamycin, clarifying the slight deviation of LCs from the vertical direction. With adding tobramycin to the system, the probability partly shifted to 30° due to the aptamer-target interaction. With increasing the number of tobramycin molecules from 5 to 40, a considerable shift in the angle probability to near 90° was achieved, highlighting the change in the direction of LCs from vertical close to horizontal. Also, there was a little probability for the angles in the range of 160°-180°, which was related to the LC molecules with a rotation of almost 180° compared to the Z axis (Figure 3B). Figure 4 shows the average of the LCs' angle respect to the Z axis for each LC molecule in the simulated systems during the MD simulation. According to Figure 4, in the control system, most of LC molecules possessed an angle of 30° and some of them had a rotation of almost 180° compared to the Z axis, proving their relatively vertical direction. With increasing the number of tobramycin, the angle of LCs enhanced from 30° to the range of 60-120°, which indicated the disruption of the LCs regularity induced by the aptamer-target interaction. For simplification in a display, the angle of LCs at the first, middle, and end of the simulation time was given in

Figures S3 and S4, which clearly shows the increase in the changes of the LCs' angle by enhancing the number of tobramycin in the system.

For further confirmation of the accuracy of the results, the lognormal distribution [65] as a continuous probability distribution of the data was applied based on the following equation:

$$Y=(A/X)*\exp(-0.5*(\ln(X/GeoMean)/\ln(GeoSD))^2)$$

in which Y and X are the probability and angle, respectively. A is related to the amplitude and area of the distribution. GeoMean and GeoSD refer to the geometric mean and geometric standard deviation factor, respectively. Table S1 represents the details and results of the lognormal distribution for the studied systems. Figure 5 indicates the angle probability of LC molecules obtained by the lognormal distribution. The results of the lognormal distribution were very close to the probability obtained from the MD output, proving the reliability of the MD results. Moreover, the R-squared values from the lognormal analysis were a confirmation for the accuracy of the MD study.

Figure 6 indicates the density of LCs along the X axis in the simulated systems at the initial (0-10 ns), middle (85-95 ns), and end (170-180 ns) of the simulation time. Obviously, the density of LCs changed with passing of the simulation time. For the control system and system containing gentamycin, the changes in the density were almost similar; and slightly increased at the end of the MD simulation. In the systems containing tobramycin, the changes in the density of LCs were significant during the MD simulation. An increase in the density of LCs was observed at the end of the MD simulation compared to that for the control system. A comparison between the density of LCs in A5T, A20T, and A40T systems highlights the significant perturbation in the LCs' alignment in the presence of more numbers of the target.

The Radial distribution function (RDF) analysis for the studied systems was obtained between the atoms of LCs and atoms of LCs with the aptamer surface. Figure S5 indicates the results, proving that the interactions of the C16-C16, N-N, and C16-N possessed no significant difference in the simulated systems. While the presence of tobramycin affected the interactions between the aptamer and LCs.

Finally, the distance between the aptamer nucleotides and tobramycin molecules was investigated in the A5T, A20T, and A40T systems (Figure 7). The distance between the target molecule and aptamer nucleotides can be a criterion for the effective interactions between them. Figure 7 clarifies that in A5T system, tobramycin 1, 4, and 5 had greater interaction with the middle nucleotides. While tobramycin 2 and 3 possessed more effective interactions with the terminal nucleotides. In A20T system, most tobramycin molecules possessed less distance

and subsequently, greater interaction with one end of the aptamer strand. In A40T system, there was more effective interaction of the target molecules with the aptamer nucleotides. As a consequence, higher interaction of tobramycin molecules with the aptamer nucleotides in A40T system induced more disruption of the vertical alignment of LCs, which was in accordance with the previous results.

4. Conclusion

In this research, we studied the potency of MD simulation to computationally design an LC-based aptasensor for the first time. As a case study, the tobramycin antibiotic has been chosen as the target molecule. 180 ns MD simulation was done for the control system, interfering system having gentamycin, and three systems with different concentrations of tobramycin (A5T, A20T, and A40T). RMSD results proved the structural stability of the simulated systems after the MD simulation. RMSF analysis indicated that the aptamer flexibility decreased in some residues with increasing the number of tobramycin, which may be due to more interaction of the aptamer with the target molecules. The basis of the LC-aptasensor is change of the vertical alignment of LCs to random in the presence of the target, due to the aptamer-target interaction. Besides, the more aptamer-target complexes, the higher disruption of the vertical arrangement of LCs is. The visualization of the last frame of the simulated systems by PyMOL software indicated that LCs were in the same direction with the vertical alignment in the control system free of tobramycin as well as the interfering system; while an increase in the number of tobramycin molecules significantly disrupted the vertical regularity of LCs. The observations were in accordance with the experimental results [6, 11]. A detailed insight was achieved by investigating the average of the angle of LCs during 180 ns. The changes in the LCs' angle were negligible in the control system and system containing gentamycin, proving an insignificant interaction of gentamycin with the aptamer. The average of the angle increased with enhancing the number of tobramycin molecules from 5 to 40 that proved the significant changes in the vertical alignment of LCs due to the great specific interaction of the aptamer with the target. With increasing the number of tobramycin molecules from 5 to 40, a great shift in the angle probability to near 90° was achieved, proving the change in the direction of LCs from vertical close to horizontal. The density of LCs in the systems containing tobramycin remarkably changed during the MD simulation. A comparison between the density of LCs in A5T, A20T, and A40T systems proved the significant irregularity in the LCs' alignment in the presence of more numbers of the target. The study confirmed the potency of MD simulation for study of the LC including biosystems. Besides, LC-based aptasensors can be

computationally designed by MD simulation and establishing a relationship between the MD-output parameters, such as the density of LCs and their angle change, with the concentration of the desired target.

Conflicts of Interest

The author(s) declare that they have no competing interests.

Acknowledgment

Financial support for this study was provided by Mashhad University of Medical Sciences. We also thank Mr. Ali Akbar Bromideh (Faculty of Mathematical Sciences, Shahid Beheshti University, Tehran, Iran) for providing statistical support.

References

1. Zavvar, T.S., et al., *CRISPR/Cas-engineered technology: Innovative approach for biosensor development.* Biosensors and Bioelectronics, 2022: p. 114501.
2. Azzouz, A., et al., *Advances in surface plasmon resonance–based biosensor technologies for cancer biomarker detection.* Biosensors and Bioelectronics, 2022. **197**: p. 113767.
3. An, J.E., et al., *Wearable cortisol aptasensor for simple and rapid real-time monitoring.* ACS sensors, 2022. **7**(1): p. 99-108.
4. Khoshbin, Z., et al., *Simultaneous detection and determination of mercury (II) and lead (II) ions through the achievement of novel functional nucleic acid-based biosensors.* Biosensors and Bioelectronics, 2018. **116**: p. 130-147.
5. Khoshbin, Z., et al., *Aptasensors as the future of antibiotics test kits-a case study of the aptamer application in the chloramphenicol detection.* Biosensors and Bioelectronics, 2018. **122**: p. 263-283.
6. Khoshbin, Z., et al., *Liquid crystal-based biosensors as lab-on-chip tools: Promising for future on-site detection test kits.* TrAC Trends in Analytical Chemistry, 2021. **142**: p. 116325.
7. Devi, M., I. Pani, and S.K. Pal, *Liquid Crystals as Signal Transducers for Sensing of Analytes Using Aptamer as Recognition Probe.* Liquid Crystals Reviews, 2022(just-accepted): p. 1-41.
8. Jang, C.-H., et al., *Using liquid crystals to report membrane proteins captured by affinity microcontact printing from cell lysates and membrane extracts.* Journal of the American Chemical Society, 2005. **127**(25): p. 8912-8913.
9. Hussain, A., A. Pina, and A. Roque, *Bio-recognition and detection using liquid crystals.* Biosensors and Bioelectronics, 2009. **25**(1): p. 1-8.
10. Wang, Y., et al., *A liquid crystal-based sensor for the simple and sensitive detection of cellulase and cysteine.* Colloids and Surfaces B: Biointerfaces, 2016. **147**: p. 100-105.
11. Rouhbakhsh, Z., A. Verdian, and G. Rajabzadeh, *Design of a liquid crystal-based aptasensing platform for ultrasensitive detection of tetracycline.* Talanta, 2020. **206**: p. 120246.
12. Wang, Y., et al., *Gold nanoparticle-based signal enhancement of an aptasensor for ractopamine using liquid crystal based optical imaging.* Microchimica Acta, 2019. **186**(11): p. 697.
13. Kim, H., Z. An, and C.-H. Jang, *Label-free optical detection of thrombin using a liquid crystal-based aptasensor.* Microchemical Journal, 2018. **141**: p. 71-79.
14. Verdian, A., Z. Rouhbakhsh, and E.J.J.o.H.M. Fooladi, *An ultrasensitive platform for PCB77 detection: New strategy for liquid crystal-based aptasensor fabrication.* 2020: p. 123531.
15. Plattner, N., et al., *Complete protein–protein association kinetics in atomic detail revealed by molecular dynamics simulations and Markov modelling.* Nature chemistry, 2017. **9**(10): p. 1005.

16. Verdian-Doghaei, A., et al., *Conformational switch of insulin-binding aptamer into G-quadruplex induced by K+ and Na+: an experimental and theoretical approach.* Journal of Biomolecular Structure and Dynamics, 2015. **33**(6): p. 1153-1163.
17. Pal, S. and S. Paul, *Conformational deviation of Thrombin binding G-quadruplex aptamer (TBA) in presence of divalent cation Sr2+: A classical molecular dynamics simulation study.* International journal of biological macromolecules, 2019. **121**: p. 350-363.
18. Monti, S., et al., *Towards the design of highly selective recognition sites into molecular imprinting polymers: a computational approach.* Biosensors and Bioelectronics, 2006. **22**(1): p. 153-163.
19. Nicholls, I.A., et al., *Theoretical and computational strategies for rational molecularly imprinted polymer design.* Biosensors and Bioelectronics, 2009. **25**(3): p. 543-552.
20. Li, M.-R., N. Zhang, and F.-S. Zhang, *Computational investigation of the conformation transitions of DNA in modified water models.* Journal of Molecular Liquids, 2018. **271**: p. 175-181.
21. Rakowska, P.W., et al., *Effect of osmolytes of different type on DNA behavior in aqueous solution. Experimental and theoretical studies.* Journal of Molecular Liquids, 2018. **271**: p. 186-201.
22. Gao, S., et al., *Study of the binding mechanism between aptamer GO18-Td and gonyautoxin 1/4 by molecular simulation.* Physical Chemistry Chemical Physics, 2016. **18**(34): p. 23458-23461.
23. Zhou, Y., et al., *Aptamer adaptive binding assessed by stilbene photoisomerization towards regenerating aptasensors.* Sensors and Actuators B: Chemical, 2018. **257**: p. 245-255.
24. Bini, A., et al., *Selection of thrombin-binding aptamers by using computational approach for aptasensor application.* Biosensors and Bioelectronics, 2011. **26**(11): p. 4411-4416.
25. Luo, D. and Y. Mu, *Computational insights into the stability and folding pathways of human telomeric DNA G-quadruplexes.* The Journal of Physical Chemistry B, 2016. **120**(22): p. 4912-4926.
26. Kim, H.W., Y.M. Rhee, and S.K. Shin, *Charge–dipole interactions in G-quadruplex thrombin-binding aptamer.* Physical Chemistry Chemical Physics, 2018. **20**(32): p. 21068-21074.
27. Phanchai, W., et al., *Insight into the molecular mechanisms of AuNP-based aptasensor for colorimetric detection: a molecular dynamics approach.* Langmuir, 2018. **34**(21): p. 6161-6169.
28. Yang, H.-W., et al., *Aptasensor designed via the stochastic tunneling-basin hopping method for biosensing of vascular endothelial growth factor.* Biosensors and Bioelectronics, 2018. **119**: p. 25-33.
29. Kim, E., C. Yang, and Y. Pak, *Free-energy landscape of a thrombin-binding DNA aptamer in aqueous environment.* Journal of chemical theory and computation, 2012. **8**(11): p. 4845-4851.
30. Yang, C., et al., *Computational Probing of Watson–Crick/Hoogsteen Breathing in a DNA Duplex Containing N1-Methylated Adenine.* Journal of chemical theory and computation, 2018. **15**(1): p. 751-761.
31. Mary, V., et al., *Experimental probing and molecular dynamics simulation of the molecular recognition of DNA duplexes by the flavonoid luteolin.* Journal of chemical information and modeling, 2017. **57**(9): p. 2237-2249.
32. Johnson, R.R., et al., *Free energy landscape of a DNA− carbon nanotube hybrid using replica exchange molecular dynamics.* Nano letters, 2009. **9**(2): p. 537-541.
33. Li, B., et al., *Finding the needle in the haystack: towards solving the protein-folding problem computationally.* Critical reviews in biochemistry and molecular biology, 2018. **53**(1): p. 1-28.
34. Moradi, S., et al., *Investigation on the interaction of acid phosphatase with putrescine using docking, simulations methods and multispectroscopic techniques.* 2020. **150**: p. 90-101.
35. Schröder, C., *Proteins in ionic liquids: current status of experiments and simulations*, in *Ionic Liquids II*. 2017, Springer. p. 127-152.
36. Zeng, X., et al., *Unfolding mechanism of thrombin-binding aptamer revealed by molecular dynamics simulation and Markov State Model.* Scientific reports, 2016. **6**.
37. Cao, L.-R., et al., *Recent Developments in Using Molecular Dynamics Simulation Techniques to Study Biomolecules.* Acta Physico-Chimica Sinica, 2017. **33**(7): p. 1354-1365.

38. Khanniche, S., et al., *Quantitative evaluation of the responses of a gravimetric gas sensor based on mesoporous functionalized silica: Application to 2, 4-DNT and TNT detection.* Sensors and Actuators B: Chemical, 2017. **248**: p. 470-480.
39. Kutnowski, N., et al., *The 3-D structure of VNG0258H/RosR–A haloarchaeal DNA-binding protein in its ionic shell.* Journal of structural biology, 2018. **204**(2): p. 191-198.
40. Masic, A., et al., *Osmotic pressure induced tensile forces in tendon collagen.* Nature communications, 2015. **6**: p. 5942.
41. Tokareva, O., et al., *Structure–function–property–design interplay in biopolymers: Spider silk.* Acta biomaterialia, 2014. **10**(4): p. 1612-1626.
42. Rigoldi, F., et al., *Molecular dynamics simulations provide insights into the substrate specificity of FAOX family members.* Molecular BioSystems, 2016. **12**(8): p. 2622-2633.
43. Ma, Q., et al., *Colorimetric aptasensors for determination of tobramycin in milk and chicken eggs based on DNA and gold nanoparticles.* Food chemistry, 2018. **249**: p. 98-103.
44. Wang, S., et al., *Bimetallic cerium/copper organic framework-derived cerium and copper oxides embedded by mesoporous carbon: Label-free aptasensor for ultrasensitive tobramycin detection.* Analytica Chimica Acta, 2019. **1047**: p. 150-162.
45. Shang, M., et al., *All-electrodeposited amorphous MoSx@ ZnO core-shell nanorod arrays for self-powered visible-light-activated photoelectrochemical tobramycin aptasensing.* Biosensors and Bioelectronics, 2019. **136**: p. 53-59.
46. Zhu, L., et al., *A new strategy for the development of efficient impedimetric tobramycin aptasensors with metallo-covalent organic frameworks (MCOFs).* Food Chemistry, 2022. **366**: p. 130575.
47. Yan, S., et al., *Label free aptasensor for ultrasensitive detection of tobramycin residue in pasteurized cow's milk based on resonance scattering spectra and nanogold catalytic amplification.* Food chemistry, 2019. **295**: p. 36-41.
48. O'Neill, M. and S.M. Kelly, *Liquid crystals for charge transport, luminescence, and photonics.* Advanced Materials, 2003. **15**(14): p. 1135-1146.
49. Pagano-Stauffer, L.A., et al. *Optical logic gates using ferroelectric liquid crystals*. in *Liquid Crystals and Spatial Light Modulator Materials*. 1986. SPIE.
50. Krieger, E. and G. Vriend, *YASARA View—molecular graphics for all devices—from smartphones to workstations.* Bioinformatics, 2014. **30**(20): p. 2981-2982.
51. DeLano, W.L., *Pymol: An open-source molecular graphics tool.* CCP4 Newsl. Protein Crystallogr, 2002. **40**(1): p. 82-92.
52. Khoshbin, Z., et al., *A novel liquid crystal-based aptasensor for ultra-low detection of ochratoxin a using a π-shaped DNA structure: Promising for future on-site detection test strips.* Biosensors and Bioelectronics, 2021. **191**: p. 113457.
53. Abraham, M.J., et al., *GROMACS: High performance molecular simulations through multi-level parallelism from laptops to supercomputers.* SoftwareX, 2015. **1-2**: p. 19-25.
54. Brooks, B.R., et al., *CHARMM: the biomolecular simulation program.* Journal of computational chemistry, 2009. **30**(10): p. 1545-1614.
55. Patel, S., A.D. Mackerell Jr, and C.L. Brooks III, *CHARMM fluctuating charge force field for proteins: II protein/solvent properties from molecular dynamics simulations using a nonadditive electrostatic model.* Journal of computational chemistry, 2004. **25**(12): p. 1504-1514.
56. Li, Z., et al., *Personal experience with four kinds of chemical structure drawing software: review on ChemDraw, ChemWindow, ISIS/Draw, and ChemSketch.* Journal of chemical information and computer sciences, 2004. **44**(5): p. 1886-1890.
57. Frisch, A., *gaussian 09W Reference.* Wallingford, USA, 25p, 2009. **470**.
58. Zoete, V., et al., *SwissParam: a fast force field generation tool for small organic molecules.* Journal of computational chemistry, 2011. **32**(11): p. 2359-2368.
59. Fletcher, R. and M.J. Powell, *A rapidly convergent descent method for minimization.* The computer journal, 1963. **6**(2): p. 163-168.
60. Bussi, G., D. Donadio, and M. Parrinello, *Canonical sampling through velocity rescaling.* The Journal of chemical physics, 2007. **126**(1): p. 014101.

61. Parrinello, M. and A. Rahman, *Polymorphic transitions in single crystals: A new molecular dynamics method.* Journal of Applied physics, 1981. **52**(12): p. 7182-7190.
62. Darden, T., D. York, and L. Pedersen, *Particle mesh Ewald: An N· log (N) method for Ewald sums in large systems.* The Journal of chemical physics, 1993. **98**(12): p. 10089-10092.
63. Li, M., et al., *Mutations in DNA-binding loop of NFAT5 transcription factor produce unique outcomes on protein–DNA binding and dynamics.* The Journal of Physical Chemistry B, 2013. **117**(42): p. 13226-13234.
64. Chakraborty, K., P. Khatua, and S. Bandyopadhyay, *Exploring ion induced folding of a single-stranded DNA oligomer from molecular simulation studies.* Physical Chemistry Chemical Physics, 2016. **18**(23): p. 15899-15910.
65. Kissell, R. and J. Poserina, *Chapter 4 - Advanced Math and Statistics*, in *Optimal Sports Math, Statistics, and Fantasy*, R. Kissell and J. Poserina, Editors. 2017, Academic Press. p. 103-135.

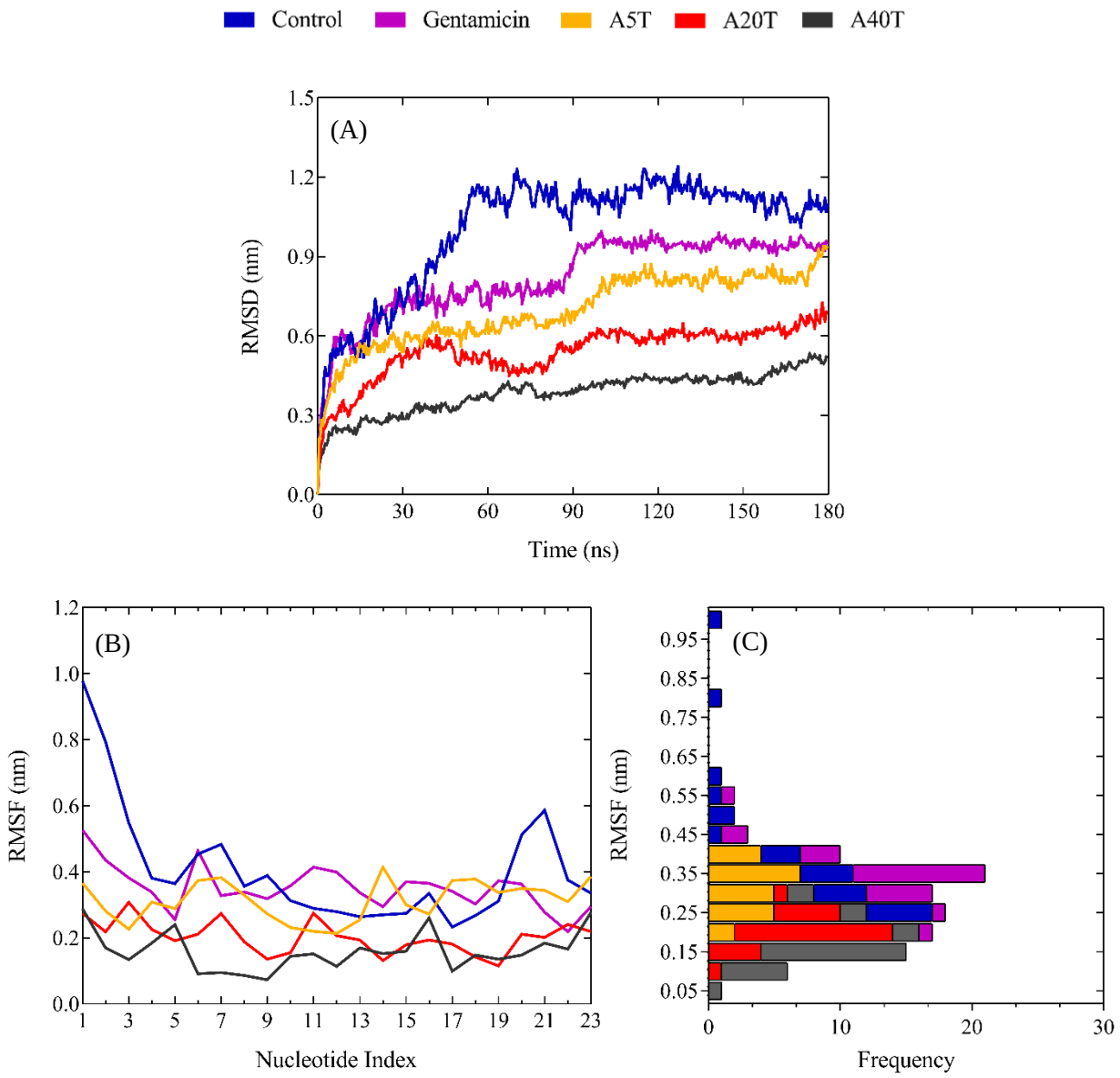

Figure 1. RMSD, RMSF, and RMSF frequency analyses (A-C) for the simulated systems during 180 ns MD simulation.

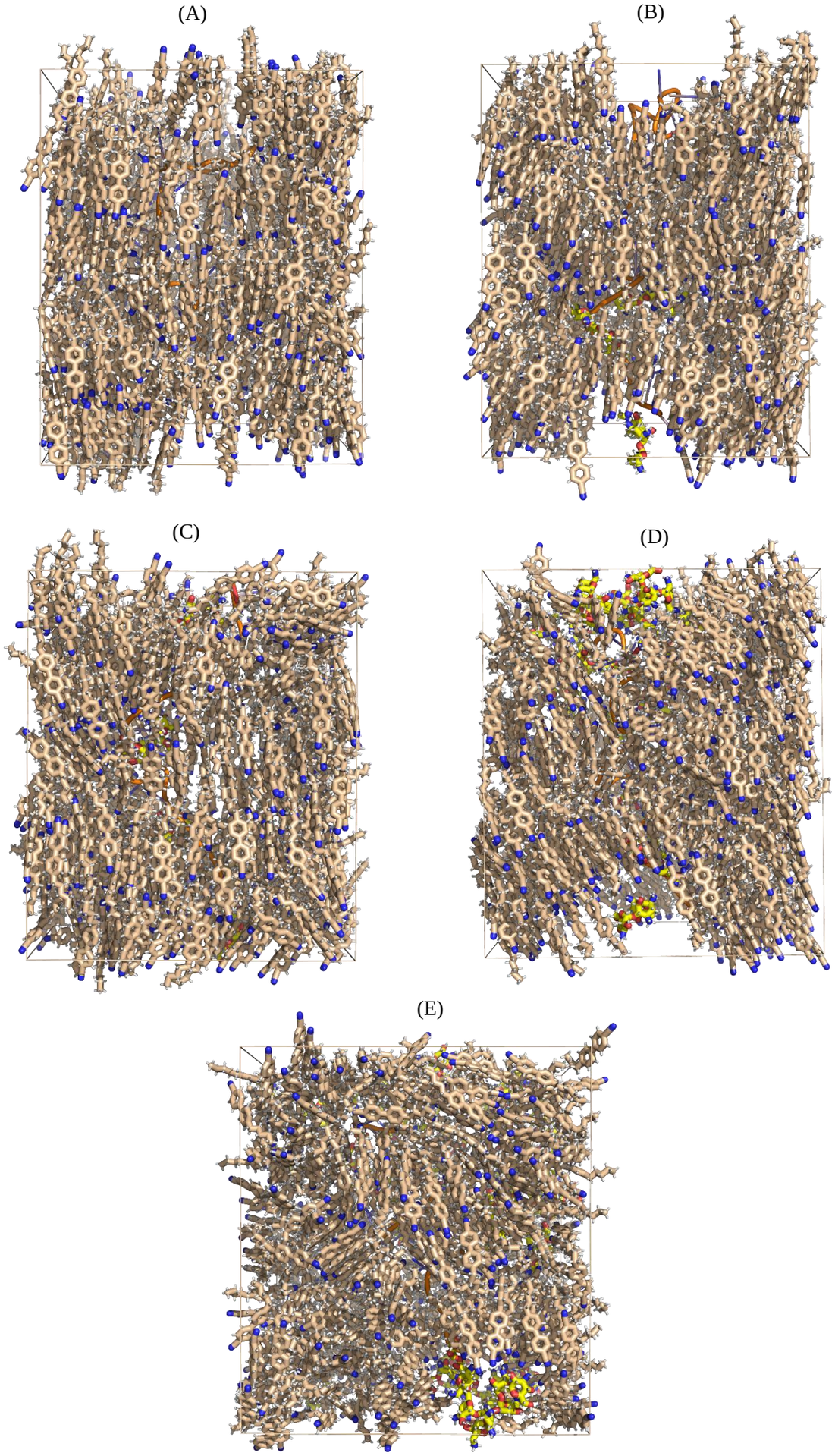

Figure 2. The situation of the LC components of the simulated systems in the last frame of the MD simulation. (A) control system free of tobramycin, (B) system containing gentamycin as the interfering compound, (C-E) systems with 5, 20, and 40 tobramycin molecules, respectively.

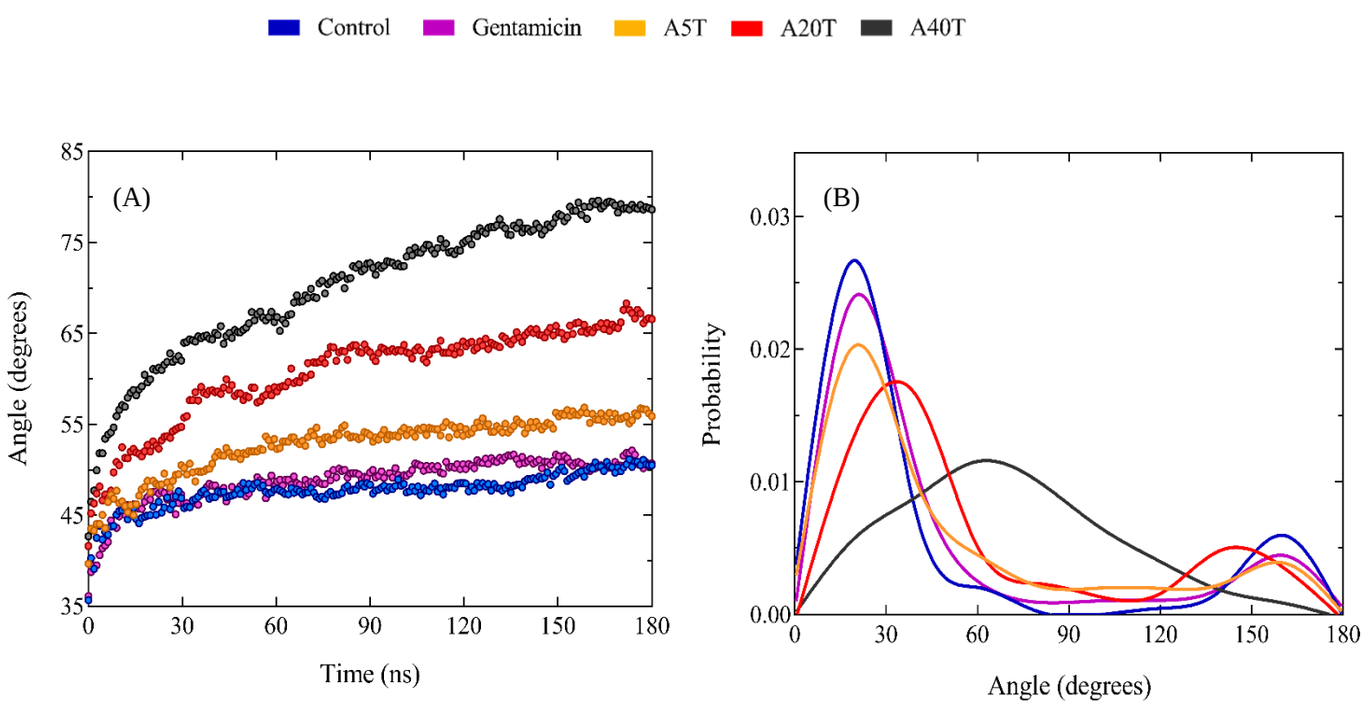

Figure 3. The average of the angles of LC molecules with respect to the Z axis of the simulation box (A) and their probability (B) during 180 ns.

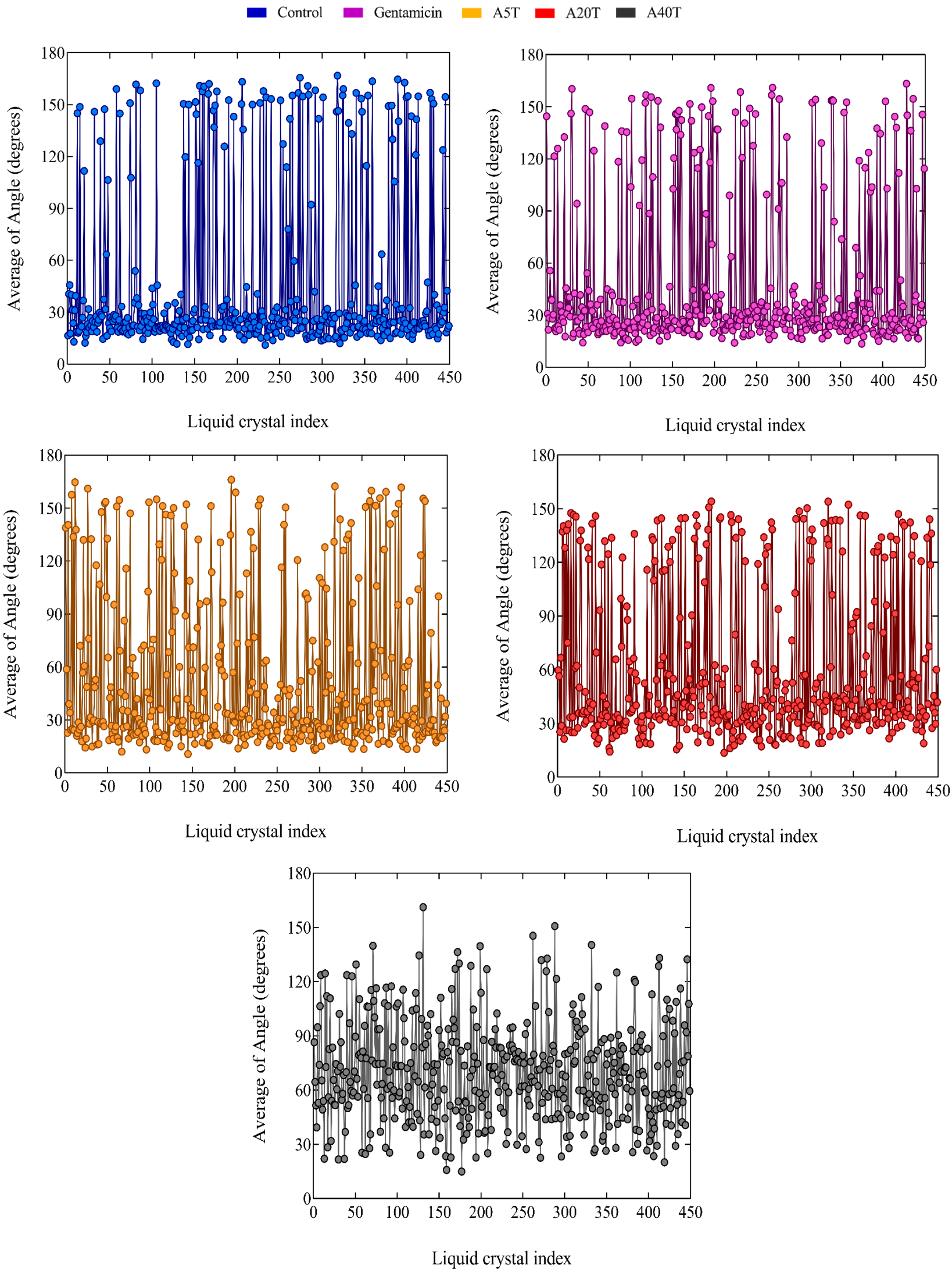

Figure 4. The average of the LCs' angle with respect to the Z axis of the simulation box for each LC molecule in the simulated systems during the MD simulation.

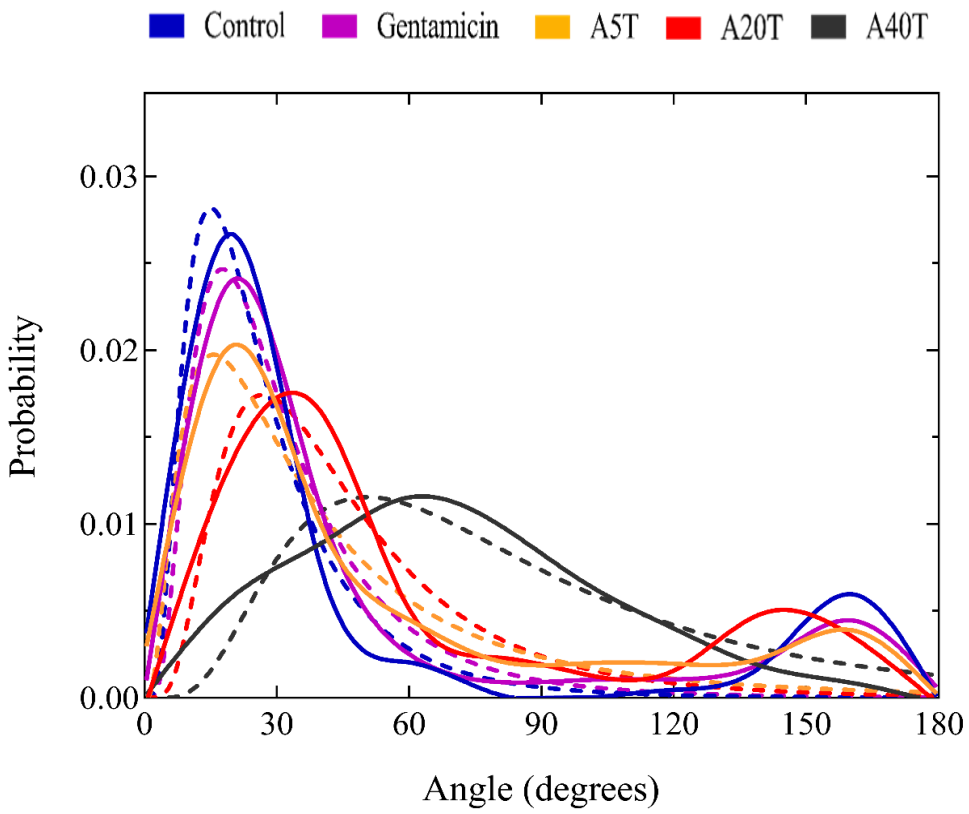

Figure 5. The angle probability of LC molecules was obtained by the lognormal distribution (dashed line) and MD simulation (solid line).

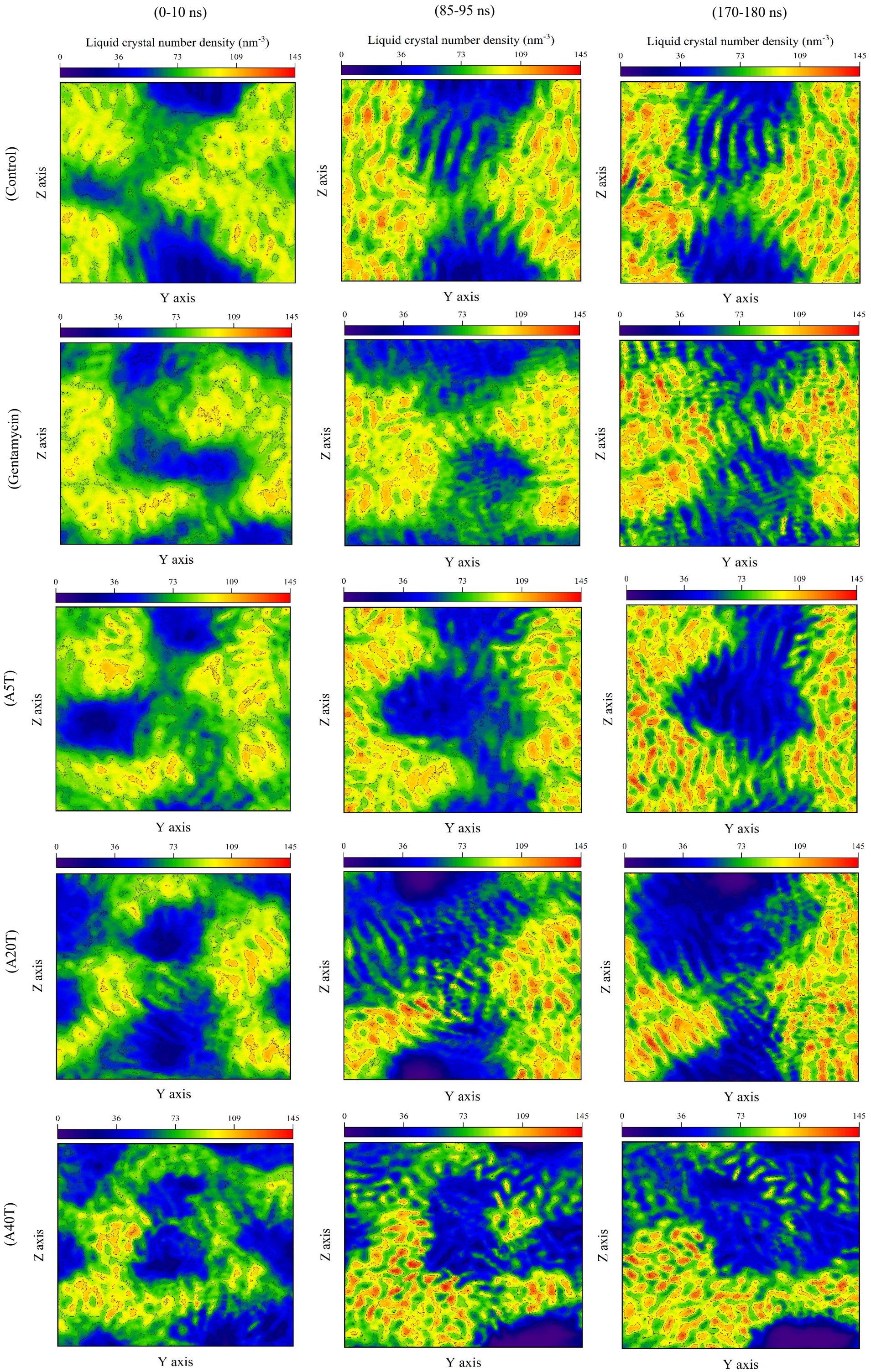

Figure 6. The density (nm^{-3}) graph of the LC molecules along the X axis in the different simulated systems at the initial, middle, and end of the simulation time.

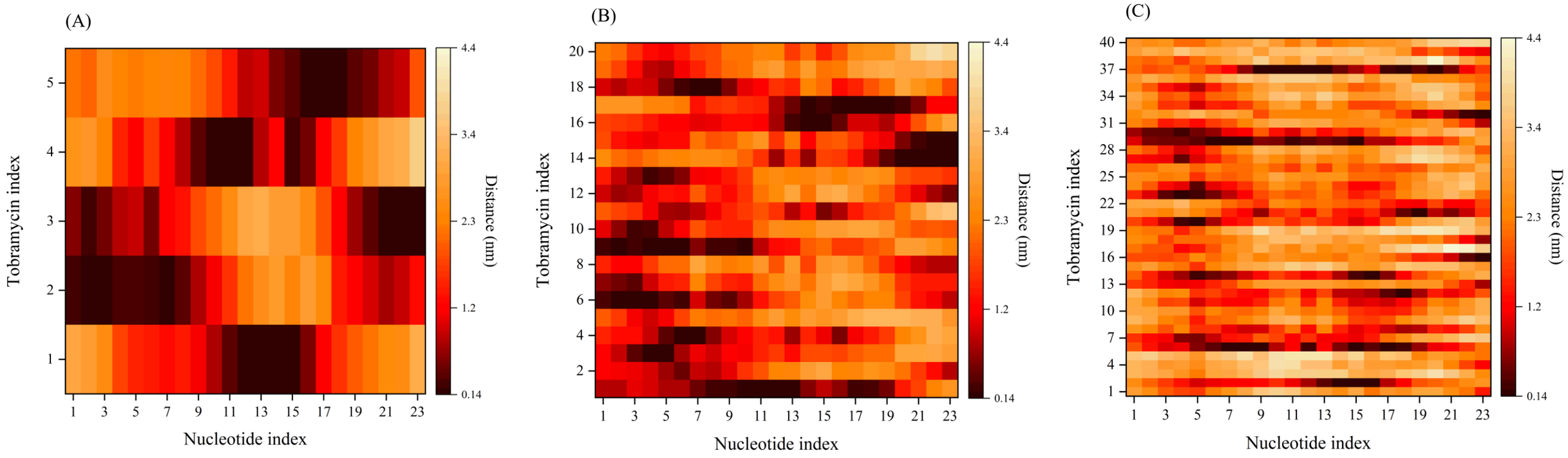

Figure 7. The distance between the tobramycin molecules and the aptamer nucleotides in the A5T, A20T, and A40T systems (A-C).

Table 1. Details of the simulated systems.

System	No. of Target	No. of LCs	Box Size (nm)	Counterion (Na^+ - Cl^-)	Time (ns)
Aptamer (Control)	0	450	7.6 × 7.6 × 9.3	22 Na^+	180 ns
Aptamer-Gentamycin	5	450	7.8 × 7.8 × 9.3	3 Cl^-	180 ns
Aptamer-Tobramycin	5	450	7.8 × 7.8 × 9.3	3 Cl^-	180 ns
	20	450	7.8 × 8.1 × 9.3	78 Cl^-	180 ns
	40	450	7.8 × 7.8 × 9.3	178 Cl^-	180 ns